Aerosol and Air Quality Research, 18: 680–692, 2018

ISSN: 1680-8584 print / 2071-1409 online
doi: 10.4209/aaqr.2017.03.0122

Chemical Compositions and Liquid Water Content of Size-Resolved Aerosol in Beijing

Jie Su, Pusheng Zhao*, Qun Dong

Institute of Urban Meteorology, China Meteorological Administration, Beijing 100089, China

ABSTRACT

For aerosol related studies, the size distribution and hygroscopicity of chemical components are very important information. In order to characterize the distributions of chemical compositions and the water absorption ability for ambient aerosols of Beijing, a MOUDI-120 sampler was used to collected size-resolved samples in three seasons. All the samples were analyzed in the laboratory for water-soluble inorganic ions and carbon fractions. The size-resolved aerosol liquid water content (ALWC) of the sampled particles was modeled by the ISORROPIA II. The distributions of the chemical compositions, the ALWC, and the charge balance conditions were all discussed for three different pollution levels. During the sampling, the aerosols in stages 6–10 (< 1.0 μm) were under relatively dry conditions due to the significant pressure drops. Three modes (condensation mode, droplet mode, and coarse mode) could be identified from the distributions of the main chemical components and the ALWC. For the droplet mode, the ammonium was not enough to balance NO_3^- and SO_4^{2-} during the heavily polluted period. The influence of relative humidity on ALWC is greater than that of the chemical compositions.

Keywords: Size-resolved; Size distribution; Chemical compositions; Aerosol liquid water content.

INTRODUCTION

Atmospheric aerosols are usually defined as four modes: nucleation mode, Aitken mode, accumulation mode and coarse mode (Hussein *et al.*, 2004, 2005). The new particles formation process generally occurs in the nucleation mode, and the new particles could grow into the Aitken mode or accumulation mode by condensation and coagulation (Wehner *et al.*, 2004; Wu *et al.*, 2007). The accumulation mode contains most of the hygroscopic chemical components, such as sulfate, nitrate, or ammonium. The particle size could be increased by several times through water uptake when under higher relative humidity (Yan *et al.*, 2008; Garland *et al.*, 2009; Ma *et al.*, 2011). Two sub-modes, named the condensation mode and the droplet mode, were also found in the accumulation mode (John, 1990, 2011).

The size distribution is one of the most fundamental parameters for aerosol chemical species. It is significantly important for studying the aerosol formation mechanism, the interaction of aerosols with radiation, or the human health effects. The cascade impactor is often used to collect size-resolved particles into several stages, and then the samples can be accurately analyzed in the laboratory for many kinds of chemical species. The new version of cascade impactors such as the MOUDI-12X (Mirco-Orifice Uniform Deposit Impactor), has more than ten stages and could achieve the minimum cutpoint of 10 nm. A great deal of labor and strict quality assurance or quality control (QA/QC) are required when using the cascade impactors for particle collection and the following laboratory analysis. Thus, the multi-stage (≥ 10 stages) cascade impactors have not been widely used yet. In previous studies, the distribution data of chemical species (especially the carbon components) obtained by multi-stage cascade impactors had not been fully presented for different seasons or different pollution levels (Yao *et al.*, 2003; Hu *et al.*, 2005; Massling *et al.*, 2009; Meier *et al.*, 2009; Guo *et al.*, 2010; Wang *et al.*, 2013). So, it is necessary to establish a set of representative distributions for several chemical species.

Among all the chemical components of the aerosol, mineral salts, secondary ions, and water-soluble organic carbon (WSOC) have strong moisture absorption properties (Gysel *et al.*, 2007; Zhao *et al.*, 2013; Liu *et al.*, 2014). The environment effects of aerosol particles, such as the extinction coefficient, the energy budget of earth atmosphere, and the secondary pollutant conversion rate, could be significantly changed because of the changes in size, density, and mass caused by the water uptake (McMurry and Wilson, 1983; Dentener *et al.*, 1996; Ravishankara, 1997; Anderson *et al.*, 2003; Seinfeld and Pandis, 2006; Kolb *et al.*, 2010;

*Corresponding author.
Tel.: +86-10-68400769
E-mail address: pszhao@ium.cn

Cheng *et al.*, 2016).

Three methods are often used to study the size-resolved aerosol hygroscopicity, and further quantitatively calculate the aerosol liquid water content (ALWC). Firstly, hygroscopic tandem differential mobility analyzer (H-TDMA) instruments are used to determine the hygroscopic growth factors (HGFs) of size-resolved aerosols. However, the observed particle size is generally smaller than 300 nm (Swietlicki *et al.*, 2008; Tan *et al.*, 2017). Secondly, the humidified nephelometer systems have also been developed to measure the light scattering enhancement factor f(RH). However, this method is unable to get the aerosol hygroscopicity in different size ranges (Koloutsou-Vakakis *et al.*, 2001; Titos *et al.*, 2014). In addition, the hygroscopic ability of ambient particles can also be indirectly calculated based on size-resolved chemical compositions by the cascade impactors (Eichler *et al.*, 2008; Meier *et al.*, 2009; Massling *et al.*, 2009; Liu *et al.*, 2014). Comparison with the results obtained by other methods, utilizing the size-resolved chemical compositions by MOUDI sampler could provide a reasonable estimation for the size-resolved HGFs (Massling *et al.*, 2009). However, the characteristics of ALWC distributions in different seasons or under different pollution levels had not been fully discussed.

Consequently, the size-resolved particles were sampled using a MOUDI sampler in the summer, autumn, and winter from 2013 to 2015. The size distribution characteristics of water-soluble ions and carbonaceous components at different pollution levels in the summer and winter had already been discussed in our published paper. In addition, the actual relative humidity in the impactors during the summer and winter sampling periods were also calculated (Zhao *et al.*, 2017). But the results for the autumn samples were not displayed in that paper. During the autumn sampling periods of this study, the $PM_{2.5}$ concentrations had been at heavy pollution level many times. Thus in this paper, the distribution characteristics of the chemical compositions are presented for the aerosol collected in the autumn.

Many aerosol thermodynamic equilibrium models have been developed to estimate the ability of particles to take up water, including EQUIL, MARS, AIM, E-AIM, SCAPE, EQUISOLV, ISORROPIA etc. (Bassett and Seinfeld, 1983; Saxena *et al.*, 1986; Wexler and Seinfeld, 1991; Jacobson *et al.*, 1996; Nenes *et al.*, 1998; Wexler and Clegg, 2002). Studies found that the ISORROPIA II model was an effective tool for ALWC estimation for water-soluble ions (Bian *et al.*, 2014; Guo *et al.*, 2015). Therefore, we utilize the ISORROPIA II model and the MOUDI results to calculate the distribution characteristics of ALWC in all these three seasons.

DATA AND MEASUREMENT

Site

The measurements were carried out on the roof of the Institute of Urban Meteorological in the Haidian district (about 36 m above the ground), which located in the northern urban area of Beijing, outside the third-ring road (39°56'N, 116°17'E). The sampling site was in the residential area, and there were no significant pollution sources nearby.

Sample Collection and Chemical Analysis

A Micro-Orifice Uniform-Deposit Impactor (MOUDI-120) was used for aerosol sampling, and the calibrated 50% cut sizes were 0.056, 0.10, 0.18, 0.32, 0.56, 1.0, 1.8, 3.1, 6.2, 9.9 and 18 μm. The MOUDI-120 could monitor the temperature inside of the cabinet and monitor the absolute pressure at the inlet and downstream of stages 6, 7, 8, 9, and 10 of the impactor every minute. In addition, the $PM_{2.5}$ mass concentrations (Metone 1020), and the ambient relative humidity were synchronously obtained by on-line monitoring.

Size-resolved sampling was performed on July 12–18, 2013, January 13–19, 2014, July 3–5, 2014, October 9–20, 2014, and January 26–28, 2015. Fifteen sets of samples were obtained for the summer time, fourteen sets of samples were collected for the autumn time, and eighteen sets for the wintertime, respectively. As mentioned in the Introduction, chemical composition data in the summer and winter had been discussed in the paper of Zhao *et al.* (2017). Thus, in this paper, the distribution characteristics discussions of the chemical components are mainly focused on the autumn results. The sampling time and average $PM_{2.5}$ concentrations for each set of samples in the autumn are given in Table 1. Except for one set of samples, all of the samples were collected from 08:00 to 19:00 for the daytime and from 20:00 to 7:00 the next day for the nighttime. The one-hour intervals were used for filter changing and nozzle plate washing with ethanol.

The hourly $PM_{2.5}$ concentrations and ambient relative humidity during the autumn sampling periods are depicted in Fig. 1. The average $PM_{2.5}$ concentration was 218.4 μg m^{-3} for the whole sampling periods (154 hours in all) with 136 hours of concentrations exceeding 75 μg m^{-3}. And the ambient relative humidity was higher than 60% in 126 hours.

Quartz fiber filters (Pallflex, 47 mm) were used for particle sampling. One-half of each quartz fiber filter was analyzed by an ion chromatography (ISC-1000, DIONEX) for water-soluble inorganic ions (Na^+, NH_4^+, K^+, Mg^{2+}, Ca^{2+}, Cl^-, NO_3^-, and SO_4^{2-}). And a 0.5cm^2 punch from a 1/4 piece of filter was analyzed by a thermal optical carbon analyzer (DRI-2001A) for OC (Organic carbon) and EC (Elemental carbon), following the IMPROVE_A protocol (Chow *et al.*, 1993, 2001, 2007).

A detailed description for the features of instruments, the procedures of pre-treatments and laboratory chemical analysis (including the quality assurance & quality control) were given in the paper of Zhao *et al.* (2017).

Methods for Calculation of Actual Relative Humidity in the Impactor

In order to obtain the accurate size distributions of ambient aerosol, the influence of the water absorption by hygroscopic particles was considered in some studies. The inner relative humidity during cascade impactors sampling was assumed to equal to the ambient relative humidity when calculating the particle Stokes diameters. The ALWC

Table 1. Sampling time and average $PM_{2.5}$ concentrations for each set of samples in the autumn.

No.	Sampling date	Start time	Duration	Average $PM_{2.5}$ (μg m^{-3})
F1	2014.10.9	8:00	11 hr	377.2
F2		20:00	11 hr	378.0
F3	2014.10.10	8:00	11 hr	362.1
F4		20:00	11 hr	294.7
F5	2014.10.16	8:00	11 hr	34.5
F6		20:00	11 hr	75.4
F7	2014.10.17	8:00	11 hr	153.0
F8		20:00	11 hr	149.2
F9	2014.10.18	8:00	11 hr	178.2
F10		20:00	11 hr	285.7
F11	2014.10.19	8:00	11 hr	265.4
F12		20:00	11 hr	199.5
F13	2014.10.20	8:00	11 hr	254.4
F14		22:00	11 hr	49.9

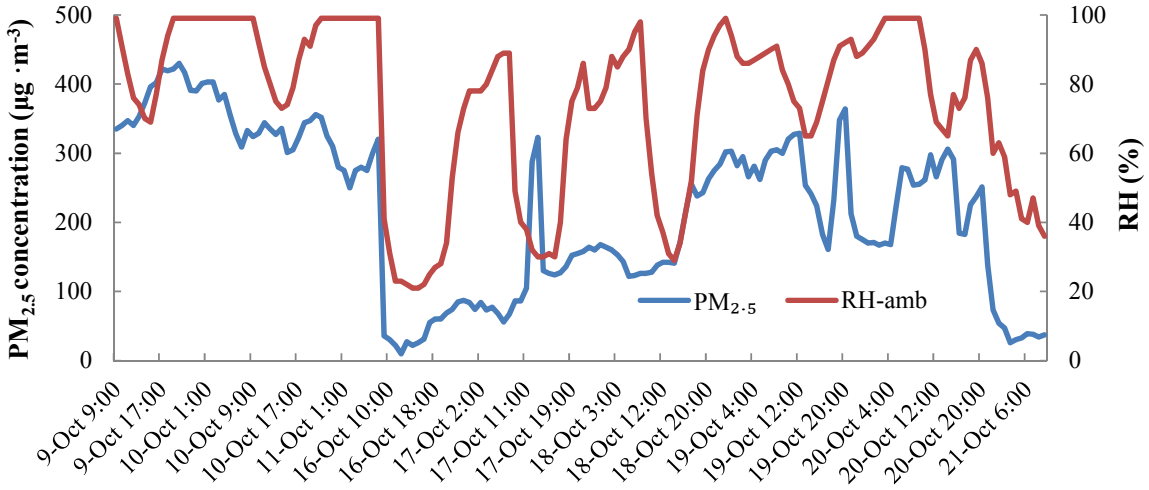

Fig. 1. $PM_{2.5}$ concentrations and relative humidity during the autumn sampling periods.

was calculated and the cutpoints of the cascade impactors were modified (Eichler *et al.*, 2008; Liu *et al.*, 2014). In practice, the pressure drops in the lower stages could significantly decrease the relative humidity. In the paper of Zhao *et al.* (2017), a new method was presented to calculate the actual relative humidity in the impactors, using Eq. (1):

$$RH_i = RH_a \cdot e_a \cdot \frac{p_i}{p_0} / e_i \quad (1)$$

where RH_i is the relative humidity in stage i of the impactors; RH_a is the ambient relative humidity; e_a and e_i are the ambient saturation water vapor pressure and saturation water vapor pressure in stage i calculated by the Goff-Gratch equation, respectively; and p_i and p_0 are the absolute pressure in stage i and stage 0 (ambient pressure), respectively.

In this paper, we also used this method to calculate the actual relative humidity in each stage of the MOUDI sampler. Table 2 shows the average relative humidity in stages 6–10 for each set of samples. The actual relative humidity in each stage of the cascade impactor was decreased with the pressure decreases. All of the relative humidity in the lower stages (< 1.0 μm) of sampler was less than 50% in the autumn, and most of them were below 40%. The actual relative humidity in the MOUDI sampler was higher than that in other two seasons due to the very high ambient relative humidity during the autumn sampling. Based on the results of all three seasons, we may come to the conclusion that the effect of aerosol moisture absorption can be ignored in most cases when collecting aerosol by multi-stage cascade impactors.

RESULTS AND DISCUSSION

Mass Concentration Size Distributions

Fig. 2 shows the scatter plots of the mass concentration size distributions for all of the analyzed species in the autumn. Three modes (condensation mode, droplet mode, and coarse mode) could be identified from the distributions of NH_4^+, NO_3^-, SO_4^{2-}, Cl^-, K^+, OC, and EC in the autumn, just like the results in the summer and winter (Zhao *et al.*, 2017). The NH_4^+, NO_3^-, SO_4^{2-}, OC, and EC were mainly distributed in droplet mode and with mass concentrations

Table 2. Average relative humidity (%) in stage 6–10 for each set of samples.

	No.	Stage 1–5 (1.0–18 μm)	Stage 6 (0.56–1.0 μm)	Stage 7 (0.32–0.56 μm)	Stage 8 (0.18–0.32 μm)	Stage 9 (0.1–0.18 μm)	Stage 10 (0.056–0.1 μm)	
Autumn	F1*	-	-	-	-	-	-	D
	F2	48.8	47.6	46.7	44.6	39.6	31.2	N
	F3	41.6	40.5	39.7	37.9	33.5	27.1	D
	F4	49.8	48.5	47.6	45.2	40.0	32.5	N
	F5	14.7	14.3	14.0	13.4	11.7	9.4	D
	F6	32.7	32.0	31.4	30.1	26.3	20.4	N
	F7	18.8	18.4	18.0	17.2	15.1	12.2	D
	F8	36.2	35.3	34.7	33.2	29.5	23.4	N
	F9	23.4	22.8	22.4	21.4	19.0	14.0	D
	F10	40.6	39.5	38.7	36.7	31.7	24.2	N
	F11	39.9	38.8	38.1	36.3	32.6	27.1	D
	F12	50.8	49.5	48.6	46.6	42.1	35.6	N
	F13	41.3	40.3	39.5	37.8	34.2	28.6	D
	F14	29.6	28.8	28.3	27.1	24.4	20.7	N

[a] D-Daytime; N-Nighttime.
[b] *Data missed.

significantly higher than other species. However, the Mg^{2+} and Ca^{2+} were primarily distributed in the coarse mode.

According to the $PM_{2.5}$ average concentration during each sampling period, all of the samples were divided into three groups: unpolluted ($PM_{2.5} \leq 75$ μg m^{-3}), polluted (75 μg m^{-3} < $PM_{2.5} \leq 150$ μg m^{-3}), and heavily polluted ($PM_{2.5} > 150$ μg m^{-3}). Two sets (F5 and F14), two sets (F6 and F8), and ten sets (F1–F4, F7, F9–F13) of autumn samples belonged to these groups, respectively.

Fig. 3 shows the average mass concentration distributions for all of the analyzed chemical species during the daytime, nighttime, unpolluted, polluted, and heavily polluted periods. There was not much difference between the distributions of each species in the nighttime and in the daytime. However, between unpolluted and polluted periods, there were considerable differences in concentration levels and size distributions.

As shown in Fig. 2, the concentrations of NO_3^-, SO_4^{2-}, NH_4^+, OC and EC for F2 were the higher than other sets, while the average $PM_{2.5}$ for F2 was also reached the highest concentration, 378.0 μg m^{-3}. The NO_3^-, SO_4^{2-}, NH_4^+, OC and EC had increased more times than other components when during the heavily polluted periods. The Mg^{2+} and Ca^{2+} are typically from fugitive or crustal dust. However, the concentration levels of Mg^{2+} and Ca^{2+} in particles sampled in heavily polluted periods did not significantly increase. This indicated that the fugitive dust was not an important source of fine particulate matter in Beijing. The study on the chemical compositions of $PM_{2.5}$ in North China also came to the same conclusion (Zhao *et al.*, 2013). During the sampling periods in all of these three seasons, the average $PM_{2.5}$ concentrations in the autumn (218.4 μg m^{-3}) was significantly higher than that in the summer (86.6 μg m^{-3}) and winter (131.3 μg m^{-3}). In the autumn, NO_3^- in heavily polluted periods was evidently higher than SO_4^{2-} and also much higher than NO_3^- in other seasons (Zhao *et al.*, 2017).

For NO_3^-, SO_4^{2-}, NH_4^+, K^+ from the autumn samples, the mass median diameters (MMDs) of the droplet mode were generally the same both under the unpolluted and the polluted periods (approximately 0.8 μm), and were smaller than the MMDs under the heavily polluted periods (about 1.0 μm). Differently, the MMDs of the droplet mode for OC and EC under the polluted and heavily polluted periods were larger than that under unpolluted periods. The samples in other two seasons also showed the same characteristics. As mentioned above, the size distributions of each species were not notably affected by the water uptake owing to the lower relative humidity in the sampler. In a word, the MMDs of accumulation mode would increase as the pollution level increases for NO_3^-, SO_4^{2-}, NH_4^+, K^+, OC, and EC, which were mainly caused by the coagulation between the small particles and the intensified surface secondary reaction. This feature can also be found in the observation of the number concentration distributions (Zhao *et al.*, 2017).

Based on the characteristics of the mass concentration distributions for each species and above analysis, we can classify these sample sets and give the representative distributions for different pollution levels or seasons. The percentages of mass concentration for each size bin to the total concentration were calculated for all species. The average mass concentration percentages for different pollution categories are listed in Table 3. The results of Na^+ and NO_2^- are not presented because they exhibited no regularity. Except for Cl^- and EC, the average distributions were highly correlated among all these three pollution levels for each species in the autumn samples.

Charge Balance Analysis

In this paper, we also calculated the molar concentrations of the positive electric charges of NH_4^+ (PEC-NH_4^+) and all of the analyzed cations (PEC-all), along with the molar concentrations of negative electric charges of all of the analyzed anions (NEC-all) for each sample. NEC-all was described by two curves (NEC-all-HSO_4^- and NEC-all-SO_4^{2-}), indicating that SO_4^{2-} was assumed to be in the form of HSO_4^- or SO_4^{2-}, respectively.

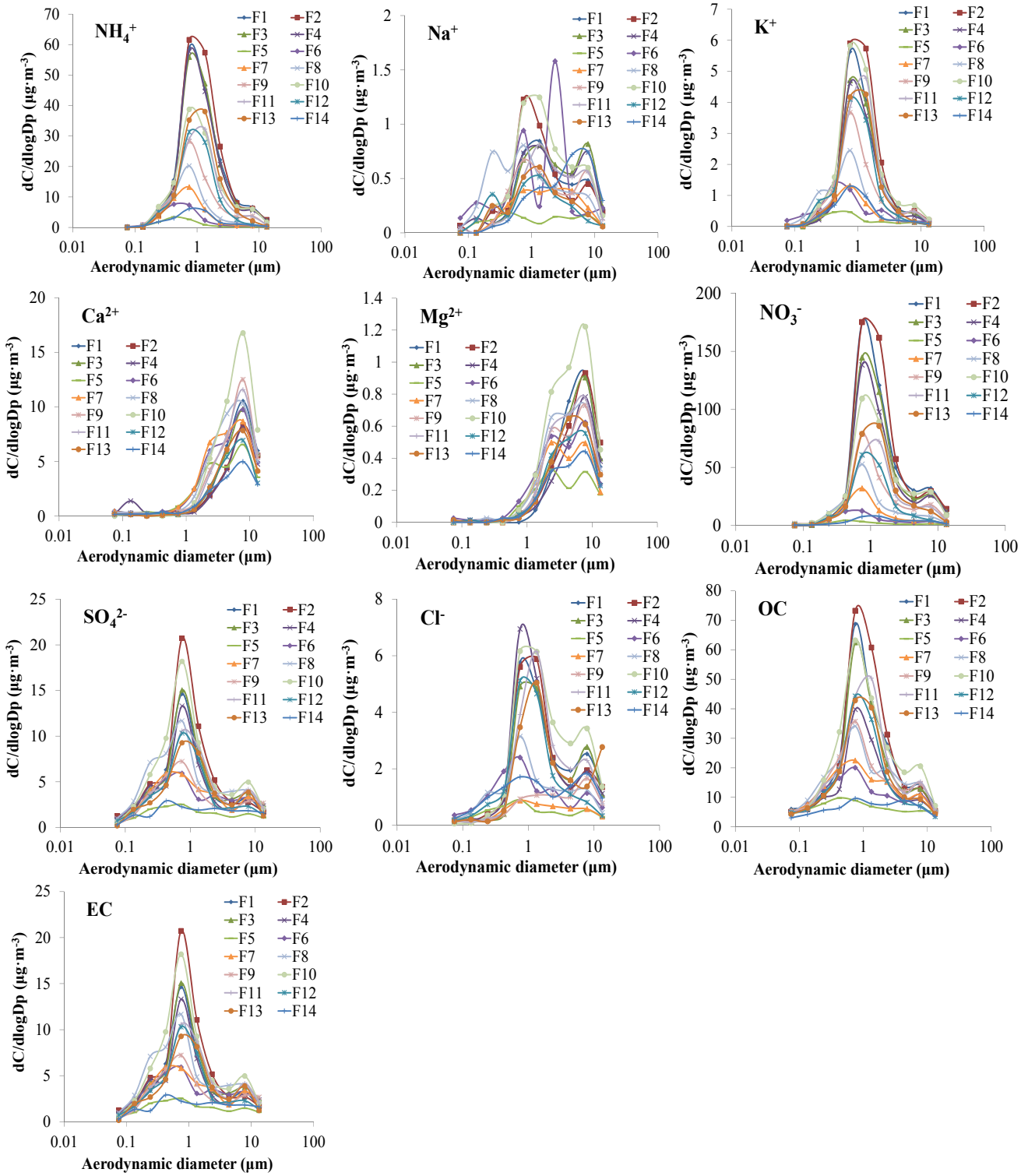

Fig. 2. Size distributions of the mass concentration for all of the analyzed species from autumn samples.

The average electric charge concentrations for different pollution levels in the autumn are displayed in Fig. 4. The PEC-NH_4^+ and PEC-all levels were both below the NEC-all level for the stage below 0.1 μm. The Aitken mode was mainly from the primary emissions of fossil fuel combustion or aged new particles. Therefore, there might be acids or other metal elements in this mode to balance the excess negative electric charges.

For the condensation mode, NEC-all was lower than PEC-NH_4^+ and PEC-all, and PEC-NH_4^+ and PEC-all were considerably close. It indicates that the cations were dominated by NH_4^+ in this mode, and the NH_4^+ was sufficient to balance the anions. The ammonium was primarily composed of NH_4NO_3 and $(NH_4)_2SO_4$.

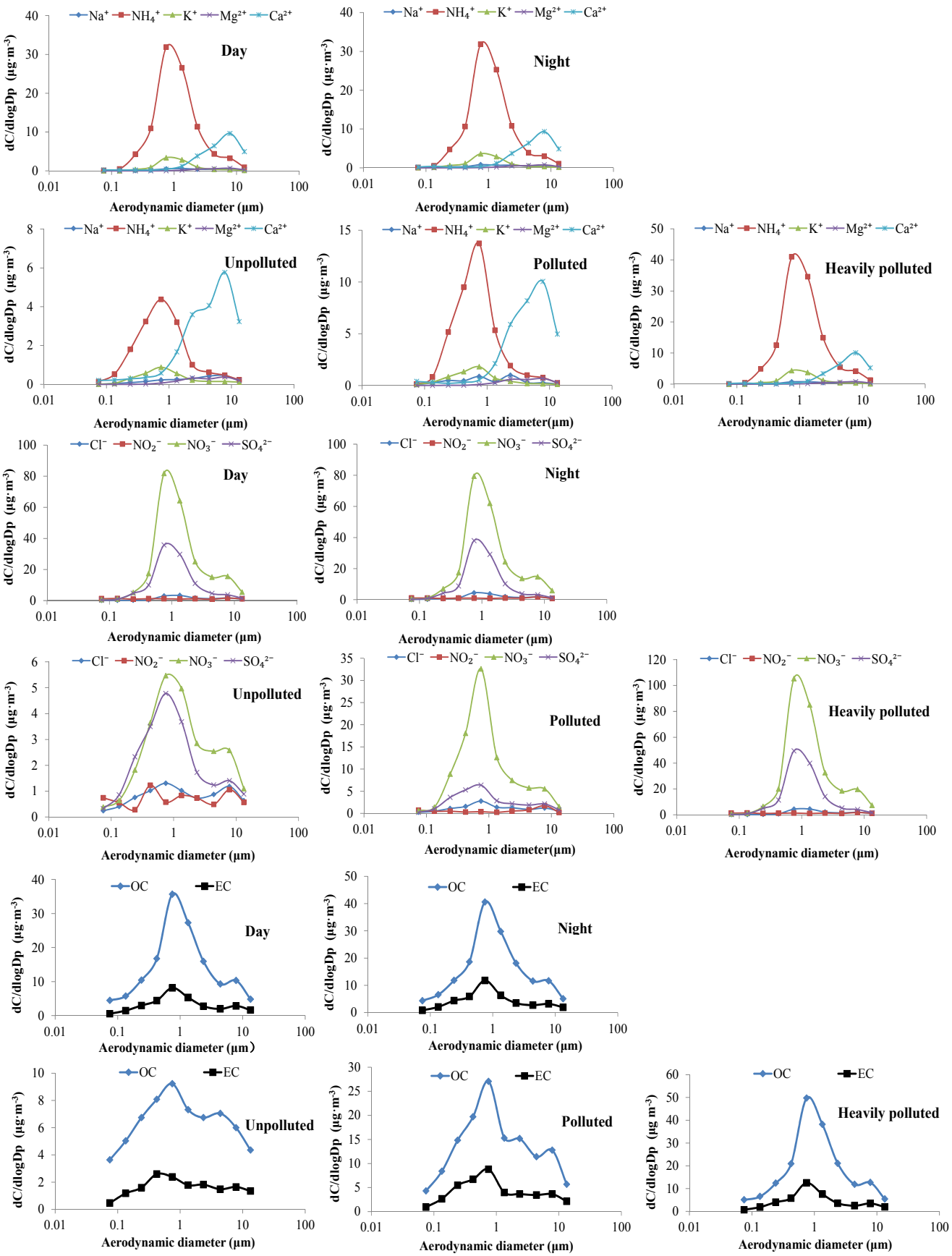

Fig. 3. Average mass concentration distributions for all of the analyzed chemical species during different periods in the autumn.

Table 3. Average mass concentration percentages for each size bin for different pollution categories in the autumn.

	Size bin (μm)	NH_4^+	K^+	Mg^{2+}	Ca^{2+}	Cl^-	NO_3^-	SO_4^{2-}	OC	EC
Unpolluted	9.9–18	1.4%	4.6%	13.8%	16.5%	7.3%	4.1%	4.5%	5.8%	8.0%
	6.2–9.9	2.7%	5.3%	26.0%	29.3%	13.5%	9.4%	6.9%	9.5%	10.3%
	3.1–6.2	3.3%	5.1%	19.4%	20.7%	9.7%	8.7%	6.0%	13.1%	9.5%
	1.8–3.1	5.7%	7.4%	22.7%	17.4%	9.2%	10.2%	8.2%	10.7%	11.2%
	1–1.8	17.4%	15.7%	12.4%	7.9%	11.8%	17.2%	16.1%	12.3%	11.2%
	0.56–1.0	27.5%	27.7%	4.9%	2.7%	16.8%	20.5%	22.1%	16.0%	15.7%
	0.32–0.56	24.0%	20.1%	0.8%	1.9%	13.0%	16.8%	17.9%	12.8%	16.8%
	0.18–0.32	13.1%	11.5%	0.0%	1.4%	9.8%	8.4%	12.1%	10.4%	9.9%
	0.1–0.18	3.8%	2.0%	0.0%	1.1%	5.4%	3.0%	4.5%	6.3%	6.2%
	0.056–0.1	1.1%	0.5%	0.0%	1.0%	3.6%	1.6%	1.8%	3.2%	1.2%
	Total	100%	100%	100%	100%	100%	100%	100%	100%	100%
Polluted	9.9–18	0.7%	2.0%	11.1%	15.1%	4.7%	1.7%	3.1%	3.4%	5.0%
	6.2–9.9	2.0%	2.8%	26.4%	30.5%	10.4%	6.3%	8.0%	9.7%	8.9%
	3.1–6.2	2.4%	3.3%	22.1%	24.7%	7.8%	5.8%	7.0%	8.6%	8.6%
	1.8–3.1	4.6%	7.3%	23.2%	17.9%	11.1%	7.6%	8.2%	11.1%	9.0%
	1–1.8	12.7%	11.5%	10.8%	6.4%	12.0%	12.5%	10.7%	11.6%	9.5%
	0.56–1.0	33.9%	29.2%	4.1%	1.7%	23.9%	31.6%	23.7%	21.6%	21.6%
	0.32–0.56	26.2%	22.7%	0.8%	0.9%	13.7%	20.9%	20.3%	15.4%	16.6%
	0.18–0.32	14.5%	13.7%	0.7%	0.6%	9.6%	10.9%	13.8%	11.3%	13.2%
	0.1–0.18	2.6%	5.6%	0.3%	0.9%	4.4%	2.0%	4.1%	5.5%	6.1%
	0.056–0.1	0.5%	2.0%	0.5%	1.2%	2.3%	0.7%	1.0%	1.7%	1.5%
	Total	100%	100%	100%	100%	100%	100%	100%	100%	100%
Heavily polluted	9.9–18	1.0%	1.1%	14.0%	19.4%	6.9%	2.2%	1.4%	2.2%	4.3%
	6.2–9.9	3.3%	3.1%	32.4%	36.9%	12.0%	6.3%	3.8%	6.6%	7.9%
	3.1–6.2	4.3%	4.0%	25.8%	23.9%	9.6%	6.2%	4.5%	6.4%	5.6%
	1.8–3.1	11.6%	10.1%	18.8%	12.1%	12.9%	10.6%	10.3%	11.5%	8.0%
	1–1.8	27.9%	30.2%	6.7%	3.2%	24.9%	27.6%	27.6%	21.8%	17.7%
	0.56–1.0	34.4%	36.4%	1.8%	1.2%	24.5%	35.3%	34.9%	28.6%	29.1%
	0.32–0.56	12.1%	10.1%	0.2%	0.6%	4.8%	8.2%	10.8%	11.6%	13.6%
	0.18–0.32	4.9%	4.3%	0.1%	0.6%	2.1%	2.6%	5.3%	6.6%	9.2%
	0.1–0.18	0.5%	0.5%	0.1%	1.3%	1.2%	0.5%	1.1%	2.8%	3.7%
	0.056–0.1	0.1%	0.2%	0.1%	0.8%	1.1%	0.3%	0.3%	1.8%	0.9%
	Total	100%	100%	100%	100%	100%	100%	100%	100%	100%

There were two cases for the droplet mode, just like the results in the other two seasons. The PEC-NH_4^+ and PEC-all were higher than NEC-all during the unpolluted and polluted periods, which was similar to the condensation mode. However, the PEC-NH_4^+ was below the NEC-all during the heavily polluted periods. It indicates that the ammonium was not enough to balance the NO_3^- and SO_4^{2-}. In this case, the ammonium might be composed of NH_4NO_3 and NH_4HSO_4. Alternatively, there might be NH_4NO_3, $(NH_4)_2SO_4$, and some acids existing because NH_4NO_3 often forms after ammonia neutralizes sulfuric acid.

For the coarse mode, these two NEC-all curves were located between the PEC-NH_4^+ and PEC-all for all of the samples. The NH_4^+ concentrations evidently decreased, and the positive electric charges might be primarily composed of metal cations. The analyzed anions were not sufficient to neutralize the analyzed cations. Therefore, there should be some soluble silicate or carbonate present.

In brief, these characteristics found by the charge balance analysis are similar to those in summer and winter (Zhao *et al.*, 2017).

Aerosol Liquid Water Content Size Distributions

The chemical composition concentration, relative humidity, and temperature are important input data of ISORROPIA II model, and also the major factors affecting ALWC. In this paper, the size-resolved ALWC in three seasons was calculated with MOUDI data. The detailed aerosol chemical information and meteorological data in the summer and the winter come from the paper of Zhao *et al.* (2017).

As indicated in Table 2, the relative humidity in each stage of impactors was different. The size-resolved ALWC in different seasons is depicted in Fig. 5 and Table 4. The blue lines (-amb) and the black lines (-impactor) on the figure represent the ALWC modeled by using the ambient relative humidity and the inner relative humidity, respectively. The abscissa of all the distributions in figures was calculated from the calibrated cutpoints of MOUDI sampler. It can be recognized as the geometric mean aerodynamic diameter of aerosols in a certain size range under relatively dry condition. However, the distributions would shift to larger diameters when the particles absorb water under ambient RH. It should be noted that the distributions of ALWC in

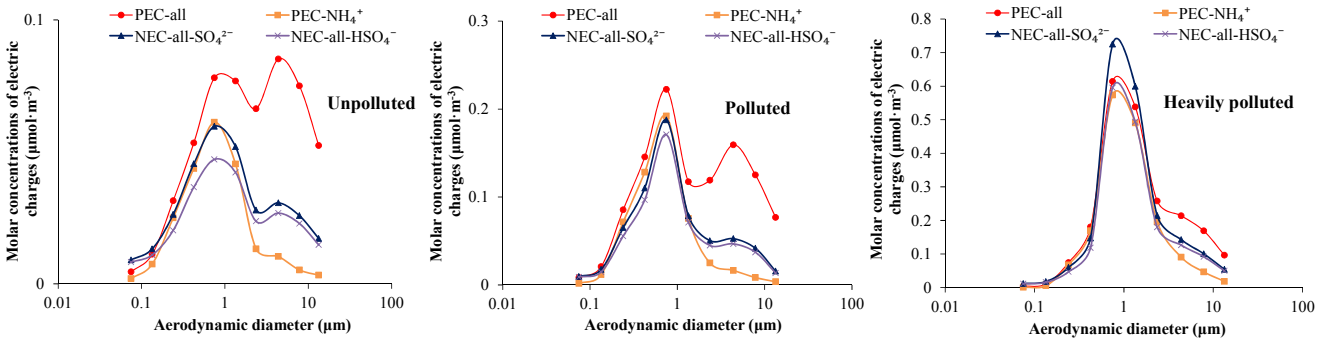

Fig. 4. Molar concentrations of positive electric charges of NH_4^+ and all of the analyzed cations, along with molar concentrations of negative electric charges of all of the analyzed anions (SO_4^{2-} assumption and HSO_4^- assumption) in the autumn.

Fig. 5 still used the original abscissa for data comparison. The ALWC modeled with the ambient relative humidity was far higher than those in the impactors, especially for the samples under the polluted and heavily polluted periods. From this, it would be a big mistake if we supposed the relative humidity in the impactors equals to the ambient relative humidity.

The ambient ALWC showed significant diurnal variations with lower values during the daytime and higher ones during the night-time. The size distributions of ALWC look like the distributions of hygroscopic chemical species, and three modes (condensation mode, droplet mode, and coarse mode) could also be identified. In most case, the ALWC in accumulation mode was largest among all these aerosol particle modes. However, the ALWC in coarse mode was at a higher level during the unpolluted periods of autumn and winter.

The $PM_{2.5}$ concentration and relative humidity were both at a higher level during the autumn sampling periods, thus the ALWC in the autumn aerosol samples were highest over these three seasons. The average $PM_{2.5}$ concentration during the summer sampling periods was lowest, the ALWC in the summer samples was higher than that in the winter due to the higher relative humidity, however. It can be concluded that the influence of relative humidity on ALWC is far more crucial than the chemical compositions. In addition, the concentration distributions of total water-soluble ions (TWSI) among these three seasons were quite similar when under the same degree of pollution.

ALWC Uncertainty

Because liquid particles have a sharply curved surface, a greater partial pressure is required to maintain mass equilibrium for a droplet. This increase in the partial pressure of vapor increases with decreasing particle size. This effect is called the Kelvin effect (Hinds, 2011). Owing to the presence of solutes, the saturation ratio required to maintain mass equilibrium for an aerosol droplet is much lower than that of the pure water droplet. Since the significant portion of the aerosol is in diameter sizes much larger than 0.1 μm, the Kelvin effect is neglected in the ISORROPIA II model (Nenes *et al.*, 1998). The recent research on the hygroscopicity of inorganic sea salt particles showed that the hygroscopic growth factor might be 6% overestimated by the ISORROPIA II model for 50nm sea salt particle under RH = 90% (Zieger *et al.*, 2017). The aerosol particles sampled by the 10th stage of MOUDI-120 sampler is 56–100 nm. Therefore, the ALWC uncertainty caused by the Kelvin effect will be neglected in this paper.

The ion concentration measurement uncertainty of ion chromatography is estimated from the variability in standards and blanks. The uncertainty of airflow rate of MOUDI sampler is 2%. The final uncertainties of ion concentrations are listed in Table 5. The uncertainty of RH measurement is 5%. The temperature and humidity were measured by one sensor, and the error of temperature has already been included in the RH. The maximum positive and negative perturbations were added to the ion concentrations and RH data, and then input the ISORROPIA II model to calculate the ALWC (Fig. 6). The maximum positive uncertainty was about 129% and the maximum negative uncertainty was 73%. We found that the higher the original ambient RH of the sample is, the greater the ALWC deviation (both of positive and negative) is, due to the exponential growth of ALWC with RH. If we only consider the samples with ambient RH lower than 90%, the maximum positive uncertainty and negative uncertainty were 38% and 21%, respectively. Therefore, the reasonable ALWC data can be obtained by using the size-resolved chemical compositions from MOUDI sample.

CONCLUSIONS

The pressure drops in the lower stages of MOUDI could significantly decreased the relative humidity of downstream. Based on the inner relative humidity and ALWC results, the effect of aerosol moisture absorption could be neglected in most cases when collecting aerosol by multi-stage cascade impactors.

Three modes (condensation mode, droplet mode, and coarse mode) could be identified from the distributions of NH_4^+, NO_3^-, SO_4^{2-}, Cl^-, K^+, OC, and EC in the autumn, just like the results in the summer and winter. The average size distributions and concentration levels of each species did not exhibit apparent differences between daytime and nighttime. For NO_3^-, SO_4^{2-}, NH_4^+, K^+, OC, and EC, the

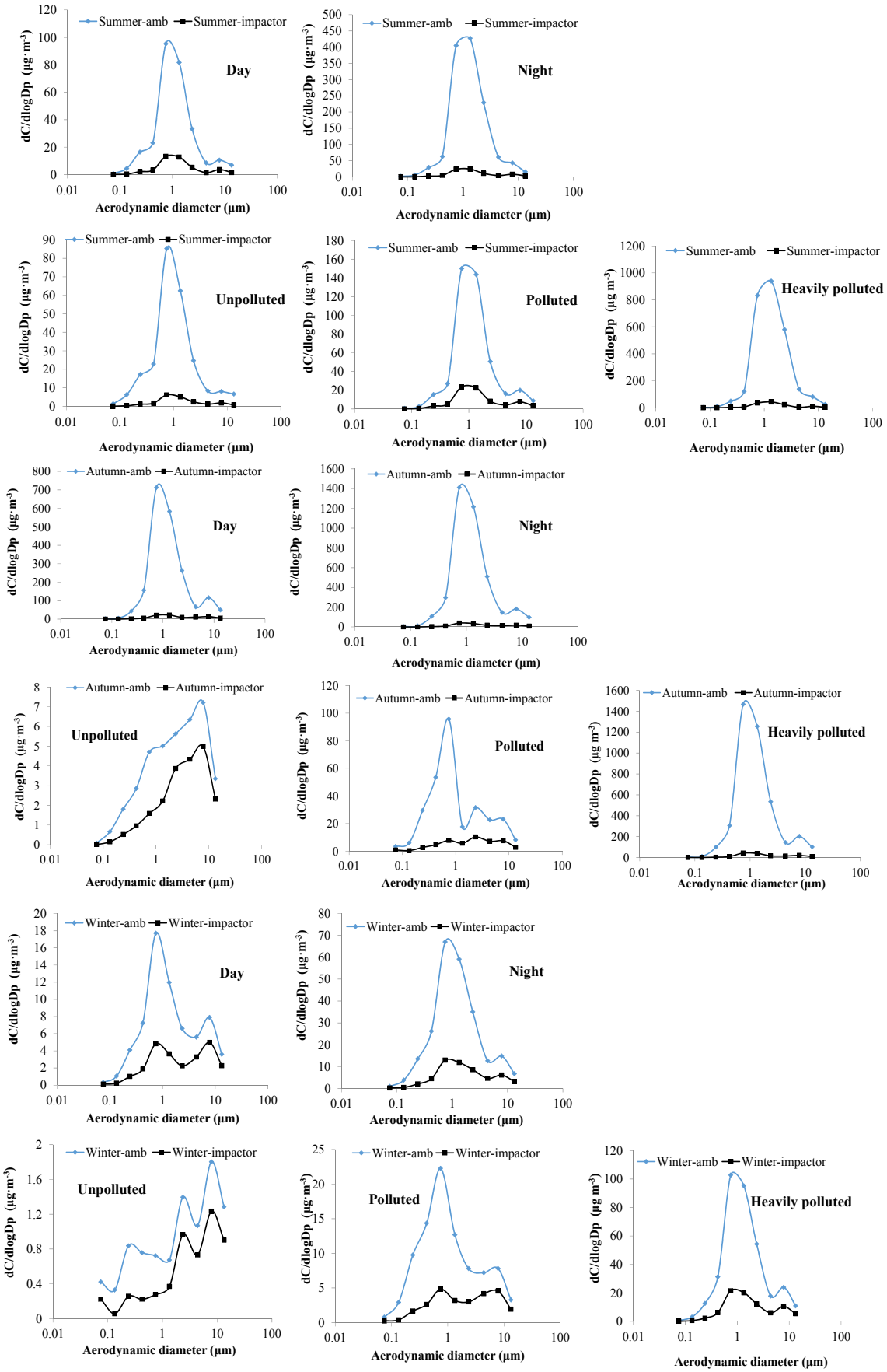

Fig. 5. Size distributions of the aerosol liquid water content in different seasons and different periods.

Table 4. Average mass concentration of ALWC and TWSI (total water soluble ions) for each sizebin in different seasons (μg m^{-3}).

dC	Sizebin		9.9–18	6.2–9.9	3.1–6.2	1.8–3.1	1–1.8	0.56–1.0	0.32–0.56	0.18–0.32	0.1–0.18	0.056–0.1	RH-amb
summer	ALWC-amb	Unpolluted	1.71	1.63	2.49	5.84	15.93	21.47	5.54	4.29	1.60	0.34	73.74%
		Polluted	2.27	4.08	4.87	11.96	36.67	37.79	6.56	3.83	0.67	0.15	77.01%
		Heavily polluted	6.53	16.64	41.73	136.83	239.73	209.58	29.31	12.26	1.87	0.49	82.55%
	TWSI	Unpolluted	0.70	1.14	1.70	2.04	4.02	4.94	1.60	1.30	0.58	0.28	-
		Polluted	1.86	3.26	5.62	9.34	22.24	22.10	4.62	2.96	0.66	0.16	-
		Heavily polluted	2.45	4.96	8.74	19.94	42.10	34.70	5.58	2.53	0.47	0.19	-
autumn	ALWC-amb	Unpolluted	0.86	1.45	1.88	1.31	1.24	1.14	0.67	0.44	0.16	0.02	38.27%
		Polluted	2.10	4.69	6.82	7.44	4.49	24.10	13.01	7.37	1.51	0.86	81.18%
		Heavily polluted	26.13	41.09	43.28	126.02	320.19	369.12	74.17	25.03	2.41	1.05	81.80%
	TWSI	Unpolluted	1.71	2.51	3.07	2.54	3.96	4.45	3.04	1.85	0.71	0.33	-
		Polluted	2.24	4.22	5.65	4.89	6.56	14.81	8.89	5.08	1.20	0.46	-
		Heavily polluted	4.47	8.45	11.68	16.38	43.24	51.74	11.21	4.35	0.73	0.33	-
winter	ALWC-amb	Unpolluted	0.33	0.37	0.32	0.33	0.17	0.18	0.18	0.21	0.08	0.11	22.56%
		Polluted	0.85	1.59	2.17	1.84	3.24	5.61	3.49	2.44	0.74	0.20	44.50%
		Heavily polluted	2.84	4.87	5.37	12.83	24.31	25.89	7.61	3.17	0.79	0.13	60.18%
	TWSI	Unpolluted	0.89	0.99	1.05	1.00	1.17	1.51	1.53	1.50	0.79	0.41	-
		Polluted	1.56	2.61	3.63	5.31	9.27	14.77	9.14	6.46	1.83	0.47	-
		Heavily polluted	3.15	6.05	9.30	18.32	32.97	39.87	12.33	5.54	1.19	0.37	-

Table 5. Uncertainties of water-soluble ions (%).

Cl^-	NO_3^-	SO_4^{2-}	Na^+	NH_4^+	K^+	Mg^{2+}	Ca^{2+}
2.4%	2.0%	2.0%	9.3%	2.0%	2.7%	4.6%	2.9%

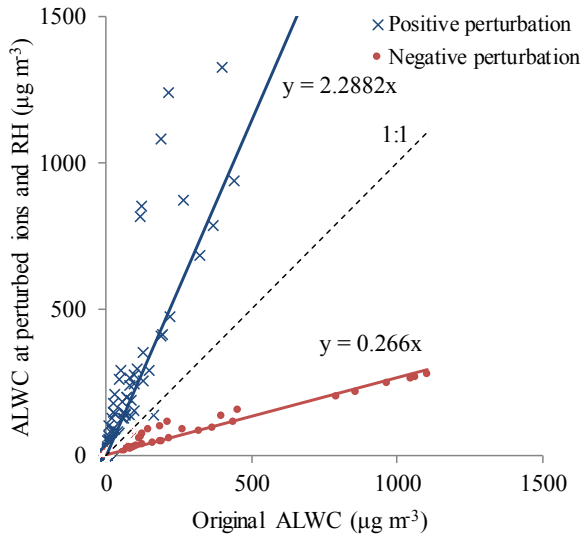

Fig. 6. Comparisons of ALWC based on artificially perturbed data and ALWC at base level.

MMDs of accumulation mode would evidently increase as the pollution increases.

The NO_3^-, SO_4^{2-}, NH_4^+, OC and EC had increased more times than other components when during the heavily polluted periods. However, the concentration levels of Mg^{2+} and Ca^{2+} in particles sampled under heavily polluted conditions did not increase significantly for all three seasons. It indicated the fugitive dust is not an important source of fine particulate matter in Beijing.

In the aerosol sampled by the stage below 0.1 μm, the cations were dominated by NH_4^+, which was not enough to balance the anions. For the condensation mode, the ammonium was primarily composed of NH_4NO_3 and $(NH_4)_2SO_4$, which was similar to that in the summer and winter. For the droplet mode, the ammonium was not enough to balance the NO_3^- and SO_4^{2-} during the heavily polluted periods.

Based on the size-resolved chemical compositions by MOUDI, the moisture absorption capacity of aerosol could be reasonably obtained. The size distributions of ALWC could be identified with three modes, just like the distributions of hygroscopic chemical species. The influence of relative humidity on ALWC was much higher than that of chemical components.

ACKNOWLEDGMENTS

This work was supported by the National Natural Science Foundation of China (41675131), the Beijing Talents Fund (2014000021223ZK49), the Beijing Natural Science Foundation (8131003), and the Beijing Municipal Science and Technology Plan Project (Z131100006113013). We also would like to thank Jianhui Wu at Nankai University for the laboratory analysis of the carbonaceous components.

REFERENCES

Anderson, T.L., Charlson, R.J., Schwartz, S.E., Knutti, R., Boucher, O., Rodhe, H. and Heintzenberg, J. (2003). Climate forcing by aerosols-a hazy picture. *Science* 300: 1103–1104.

Bassett, M. and Seinfeld, J.H. (1983). Atmospheric equilibrium model of sulfate and nitrate aerosols. *Atmos. Environ.* 17: 2237–2252.

Bian, Y.X., Zhao, C.S., Ma, N., Chen, J. and Xu, W.Y. (2014). A study of aerosol liquid water content based on hygroscopicity measurements at high relative humidity in the North China Plain. *Atmos. Chem. Phys.* 14: 6417–6426.

Cheng, Y.F., Zheng, G.J., Wei, C., Mu, Q., Zheng, B., Wang, Z.B., Gao, M., Zhang, Q., He, K.B., Carmichael, G., Pöschl, U. and Su, H. (2016). Reactive nitrogen chemistry in aerosol water as a source of sulfate during haze events in China. *Sci. Adv.* 2: e1601530.

Chow, J.C., Watson, J.G., Pritchett, L.C., Pierson, W.R., Frazier, C.A. and Purcell, R.G. (1993). The DRI thermal/optical reflectance carbon analysis system: Description, evaluation and application in U.S. air quality studies. *Atmos. Environ.* 27: 1185–1201.

Chow, J.C., Watson, J.G., Crow, D., Lowenthal, D.H. and Merrifield, T. (2001). Comparison of IMPROVE and NIOSH carbon measurements. *Aerosol Sci. Technol.* 34: 23–34.

Chow, J.C., Watson, J.G., Antony Chen, L.W., Oliver Chang, M.C., Robinson, N. F., Trimble, D. and Kohl, S. (2007). The IMPROVE A temperature protocol for thermal/optical carbon analysis: Maintaining consistency with a long-term database. *J. Air Waste Manage. Assoc.* 57: 1014–1023.

Dentener, F.J., Carmichael, G.R., Zhang, Y., Lelieveld, J. and Crutzen, P.J. (1996). Role of mineral aerosol as a reactive surface in the global troposphere. *J. Geophys. Res.* 101: 22869–22889.

Eichler, H., Cheng, Y.F., Birmili, W., Nowak, A., Wiedensohler, A., Brüggemann, E., Gnauk, T., Herrmann, H., Althausen, D., Ansmann, A., Engelmann, R., Tesche, M., Wendisch, M., Zhang, Y.H., Hu, M., Liu, S. and Zeng, L.M. (2008). Hygroscopic properties and extinction of aerosol particles at ambient relative humidity in South-Eastern China. *Atmos. Environ.* 42: 6321–6334.

Garland, R.M., Schmid, O., Nowak, A., Achtert, P., Wiedensohler, A., Gunthe, S.S., Takegawa, N., Kita, K., Kondo, Y., Hu, M., Shao, M., Zeng, L.M., Zhu, T., Andreae, M.O. and Pöschl U. (2009). Aerosol optical properties observed during Campaign of Air Quality Research in Beijing 2006 (CAREBeijing-2006):

Characteristic differences between the inflow and outflow of Beijing city air. *J. Geophys. Res.* 114: D00G04.

Guo, H., Xu, L., Bougiatioti, A., Cerully, K.M., Capps, S.L., Hite, J.R., Jr., Carlton, A.G., Lee, S.H., Bergin, M.H., Ng, N.L., Nenes, A. and Weber, R.J. (2015). Fine-particle water and pH in the southeastern United States. *Atmos. Chem. Phys.* 15: 5211–5228.

Guo, S., Hu, M., Wang, Z.B., Slanina, J. and Zhao Y.L. (2010). Size-resolved aerosol water-soluble ionic compositions in the summer of Beijing: Implication of regional secondary formation. *Atmos. Chem. Phys.* 10: 947–959.

Gysel, M., Crosier, J., Topping, D.O., Whitehead, J.D., Bower, K.N., Cubison, M.J., Williams, P.I., Flynn, M.J., McFiggans, G.B. and Coe, H. (2007). Closure study between chemical compostion and hygroscopic growth of aerosol particles during TORCH$_2$. *Atmos. Chem. Phys.* 7: 6131–6144.

Hinds, W.C. (2011). Physical and chemical processes in aerosol systems, In *Aerosol measurement*, 3rd edition, Kulkarni, P., (Ed.), John Wiley & Sons, Inc, Hoboken, pp. 31–40.

Hu, M., Zhao, Y.L., He, L.Y., Huang, X.F., Tang, X.Y., Yao, X.H. and Chan, C.K. (2005). Mass size distribution of Beijing particulate matters and its inorganic water-soluble ions in winter and summer. *Environ. Sci.* 26: 1–6 (in Chinese).

Hussein, T., Dal Maso, M., Petäjä, T., Koponen, I.K., Paatero, P., Aalto, P.P., Hämeri, K. and Kulmala, M. (2005). Evaluation of an automatic algorithm for fitting the particle number size distributions. *Boreal Environ. Res.* 10: 337–355.

Hussein, T., Puustinen, A., Aalto, P.P., Mäkelä, J.M., Hämeri, K. and Kulmala, M. (2004). Urban aerosol number size distributions. *Atmos. Chem. Phys.* 4: 391–411.

Jacobson, M.Z., Tabazadeh, A. and Turco, R.P. (1996). Simulating equilibrium within aerosols and nonequilibrium between gases and aerosols. *J. Geophys. Res.* 101: 9079–9091.

John, W. (2011). Size distribution characteristics of aerosols, In *Aerosol measurement*, 3rd edition, Kulkarni, P. (Ed.), John Wiley & Sons, Inc, Hoboken, pp. 41–54.

John, W., Wall, S.M., Ondo, J.L. and Winklmayr, W. (1990). Modes in the size distributions of atmospheric inorganic aerosol. *Atmos. Environ.* 24: 2349–2359.

Kolb, C.E., Cox, R.A., Abbatt, J.P.D., Ammann, M., Davis, E.J., Donaldson, D.J., Garrett, B.C., George, C., Griffiths, P.T., Hanson, D.R., Kulmala, M., McFiggans, G., Pöschl, U., Riipinen, I., Rossi, M.J., Rudich, Y., Wagner, P.E., Winkler, P.M., Worsnop, D.R. and O'Dowd, C.D. (2010). An overview of current issues in the uptake of atmospheric trace gases by aerosols and clouds. *Atmos. Chem. Phys.* 10: 10561–10605.

Koloutsou-Vakakis, S., Carrico, C.M., Kus, P., Rood, M.J., Li, Z., Shrestha, R., Ogren, J.A., Chow, J.C. and Watson, J.G. (2001). Aerosol properties at a midlatitude northern hemisphere continental site. *J. Geophys. Res.* 106: 3019–3032.

Liu, H.J., Zhao, C.S., Nekat, B., Ma, N., Wiedensohler, A., Van Pinxteren, D., Spindler, G., Müller, K. and Herrmann, H. (2014). Aerosol hygroscopicity derived from size-segregated chemical composition and its parameterization in the North China Plain. *Atmos. Chem. Phys.* 14: 2525–2539.

Ma, N., Zhao, C.S., Nowak, A., Müller, T., Pfeifer, S., Cheng, Y.F., Deng, Z.Z., Liu, P.F., Xu, W.Y., Ran, L., Yan, P., Göbel, T., Hallbauer, E., Mildenberger, K., Henning, S., Yu, J., Chen, L.L., Zhou, X.J., Stratmann, F. and Wiedensohler, A. (2011). Aerosol optical properties in the North China Plain during HaChi campaign: An in-situ optical closure study. *Atmos. Chem. Phys.* 11: 5959–5973.

Massling, A., Stock, M., Wehner, B., Wu, Z.J., Hu, M., Brüggemann, E., Gnauk, T., Herrmann, H. and Wiedensohler, A. (2009). Size segregated water uptake of the urban submicrometer aerosol in Beijing. *Atmos. Environ.* 43: 1578–1589.

McMurry, P.H. and Wilson, J.C. (1983). Droplet phase (Heterogeneous) and gas phase (homogeneous) contributions to secondary ambient aerosol formation as functions of relative humidity. *J. Geophys. Res.* 88: 5101–5108.

Meier, J., Wehner, B., Massling, A., Birmili,W., Nowak, A., Gnauk, T., Brüggemann, E., Herrmann, H., Hu, M. and Wiedensohler, A. (2009). Hygroscopic growth of urban aerosol particles in Beijing (China) during wintertime: A comparison of three experimental methods. *Atmos. Chem. Phys.* 9: 6865–6880.

Nenes, A., Pandis, S. and Pilinis, C. (1998). ISORROPIA: A new thermodynamic equilibrium model for multiphase multicomponent inorganic aerosols. *Aquat. Geochem.* 4: 123–152.

Ravishankara, A.R. (1997). Heterogeneous and multiphase chemistry in the troposphere. *Science* 276: 1058–1065.

Saxena, P., Belle Hudischewskyj, A., Seigneur, C. and Seinfeld, J.H. (1986). A comparative study of equilibrium approaches to the chemical characterization of secondary aerosols. *Atmos. Environ.* 20: 1471–1483.

Seinfeld, J.H. and Pandis, S.N. (2006). *Atmospheric chemistry and physics*, John Wiley & Sons, Inc, Hoboken.

Swietlicki, E., Hansson, H.C., Hämeri, K., Svenningsson, B., Massling, A., McFiggans, G., McMurry, P.H., Petäjä, T., Tunved, P., Gysel, M., Topping, D., Weingartner, E., Baltensperger, U., Rissler, J., Wiedensohler, A. and Kulmala, M. (2008). Hygroscopic properties of submicrometer atmospheric aerosol particles measured with H-TDMA instruments in various environments - A review. *Tellus B* 60: 432–469.

Tan, H.B., Cai, M.F., Fan, Q., Liu, L., Li, F., Chan, P.W., Deng, X.J. and Wu, D. (2017). An analysis of aerosol liquid water content and related impact factors in Pearl River Delta. *Sci. Total Environ.* 579: 1822–1830.

Titos, G., Jefferson, A., Sheridan, P.J., Andrews, E., Lyamani, H., Alados-Arboledas, L. and Ogren, J.A. (2014). Aerosol light-scattering enhancement due to water uptake during TCAP campaign. *Atmos. Chem. Phys.* 14: 7031–7043.

Wang, X.F., Wang, T., Pathak, R.K., Hallquist, M., Gao, X.M., Nie, W., Xue, L.K., Gao, J., Gao, R., Zhang, Q.Z.,

Wang, W.X., Wang, S.L., Chai, F.H. and Chen Y.Z. (2013). Size distributions of aerosol sulfates and nitrates in Beijing during the 2008 Olympic Games: Impacts of pollution control measures and regional transport. *Adv. Atmos. Sci.* 30: 341–353.

Wehner, B., Wiedensohler, A., Tuch, T.M., Wu, Z.J., Hu, M., Slanina, J. and Kiang, C.S. (2004). Variability of the aerosol number size distribution in Beijing, China: New particle formation, dust storms, and high continental background. *Geophys. Res. Lett.* 31: 217–244.

Wexler, A.S. and Seinfeld, J.H. (1991). Second-generation inorganic aerosol model. *Atmos. Environ.* 25: 2731–2748.

Wexler, A.S. and Clegg, S.L. (2002). Atmospheric aerosol models for systems including the ions H^+, NH_4^+, Na^+, SO_4^{2-}, NO_3^-, Cl^-, Br^-, and H_2O. *J. Geophys. Res.* 107: D14.

Wu, Z.J., Hu, M., Liu, S., Wehner, B., Bauer, S., Ma ßling, A., Wiedensohler, A., Petäjä, T., Dal Maso, M. and Kulmala, M. (2007). New particle formation in Beijing: China Statistical analysis of a 1-year data set. *J. Geophys. Res.* 112: D09209.

Yan, P., Tang, J., Huang, J., Mao, J.T., Zhou, X.J., Liu, Q., Wang, Z.F. and Zhou, H.G. (2008). The measurement of aerosol optical properties at a rural site in Northern China. *Atmos. Chem. Phys.* 8: 2229–2242.

Yao, X.H., Lau, A.P.S., Fang, M., Chan, C.K. and Hu, M. (2003). Size distributions and formation of ionic species in atmospheric particulate pollutants in Beijing, China: 1-inorganic ions. *Atmos. Environ.* 37: 2991–3000.

Zhao, P.S., Dong, F., He, D., Zhao, X.J., Zhang, X.L., Zhang, W.Z., Yao, Q. and Liu H.Y. (2013). Characteristics of concentrations and chemical compositions for $PM_{2.5}$ in the region of Beijing, Tianjin, and Hebei, China. *Atmos. Chem. Phys.* 13: 4631–4644.

Zhao, P.S., Chen Y.N. and Su, J. (2017). Size-resolved carbonaceous components and water-soluble ions measurements of ambient aerosol in Beijing. *J. Environ. Sci.* 54: 298–313.

Zieger, P., Väisänen, O., Corbin, J.C., Partridge, D.G., Bastelberger, S., Mousavi-Fard, M., Rosati, B., Gysel, M., Krieger, U.K., Leck, C., Nenes, A., Riipinen, I., Virtanen, A. and Salter, M.E. (2017). Revising the hygroscopicity of inorganic sea salt particles. *Nat. Commun.* 8: 15883.

Received for review, April 16, 2017
Revised, October 16, 2017
Accepted, November 9, 2017